# Interstitial iron impurities at grain boundaries in silicon: A first-principles study

Benedikt Ziebarth,[1,2,*] Matous Mrovec,[1] Christian Elsässer,[1] and Peter Gumbsch[1,2]
[1]*Fraunhofer Institut für Werkstoffmechanik IWM, Wöhlerstrasse 11, 79108 Freiburg, Germany*
[2]*Karlsruher Institut für Technologie, Institut für Angewandte Materialien (IAM-CMS), Engelbert-Arnold-Strasse 4, 76131 Karlsruhe, Germany*
(Received 17 October 2014; published 14 January 2015)

Iron impurities have a negative effect on the efficiency of silicon-based solar cells because they act as trapping centers for charge carriers. Various processing techniques have been applied to improve the efficiency by passivating the Fe contaminants. For instance, internal gettering exploits the attractive interaction between interfaces and the diffusing Fe atoms. Therefore, it is interesting and important to develop a fundamental understanding of mechanisms for this interaction. In this work, we employ density functional theory to study the electronic structure and the segregation behavior of impurity atoms at grain boundaries (GBs). The investigated set of symmetrical tilt or twist GBs in Si provides a variety of interface orientations and structures at the atomic scale. Our results suggest that segregation of interstitial Fe occurs only at specific sites at some of these GBs, e.g., the Σ 3 (112) GBs and Σ 3 (110) GBs. However, there seems to be no obvious relation between the computed segregation energies and the local coordination and electronic structure at the segregation sites. Hence, the thermodynamics of interstitial Fe at GBs in Si is determined by rather subtle features of structure and bonding.

DOI: 10.1103/PhysRevB.91.035309 PACS number(s): 61.72.Mm, 88.40.jj, 64.75.Qr, 73.20.Hb

## I. INTRODUCTION

Multicrystalline silicon (mc-Si) is the most economical feedstock material for Si-based solar cells. Due to the very challenging market situation for solar-cell production, companies are forced to reduce the costs of their solar modules by using cheaper feedstock materials like metallurgical silicon [1]. These savings usually come with the disadvantage of larger amounts of metallic impurities in the material that cause electrical efficiency losses due to their action as recombination centers [2–6] or due to the formation of precipitates [7]. Among these metallic impurities iron is known to have a strong detrimental effect on the efficiency of the solar cell [8]. Different processing techniques are applied for the passivation of Fe contaminants in order to improve the solar-cell efficiency. For instance, internal gettering exploits the attractive interaction between grain boundaries (GBs) in the mc-Si and the diffusing Fe atoms [9–13]. Therefore, it is interesting and important to develop a fundamental understanding of the mechanism for this interaction. The segregation of Fe atoms and the precipitation of Fe silicide particles at GBs have been examined by various experimental studies using methods like photoluminescence (PL) spectroscopy [14–16] and electron-beam-induced current (EBIC) measurements [17,18] in combination with transmission electron microscopy (TEM) [19–21], scanning electron microscopy (SEM) [17,19,22], and electron backscatter diffraction (EBSD) [17,19,22]. All these studies indicate that the segregation of Fe at GBs in Si strongly depends both on the misorientation of grains, often denoted by the Σ value of the coincidence-site lattice [23], and on the inclination of the GBs, as denoted by the Miller indices ($hkl$) of the interface plane. For instance, it was shown that the Σ 3 (111) GB is not gettering Fe, whereas Σ 3 (112) and Σ 3 (110) GBs contain large amounts of segregated Fe [17,19,24]. Hence, to characterize the gettering efficiency of a GB solely by its Σ value is not sufficient.

The behavior of impurity Fe atoms in Si bulk crystals has already been studied extensively both theoretically and experimentally. The Fe impurities in bulk Si occupy tetrahedral interstitial sites in the diamond structure of crystalline Si. In $p$-type doped Si the Fe is positively charged ($Fe^{+}$); in $n$-type or nondoped Si the Fe remains uncharged ($Fe^{0}$) [2,25]. Interstitial Fe creates a deep donor level at 0.4 eV above the valence band edge of bulk Si, which causes the photoinduced charge carriers (electrons and holes) to recombine easily [2]. The electronic behavior of Fe in bulk Si was successfully explained by Ludwig and Woodbury, who showed that the two 4$s$ electrons of the bcc Fe atom are both transferred into the 3$d$ bands when the Fe atom is embedded in the Si crystal [26]. This simple model is in very good agreement with electron paramagnetic-resonance measurements and first-principles electronic-structure calculations [25,27].

In this study, we investigate interstitial Fe impurities and their interaction with a set of low-Σ symmetrical (tilt or twist) GBs by means of first-principles density functional theory (DFT) calculations. The set of investigated GBs provides a variety of interface orientations and structures at the atomic scale. Therefore, we believe that our results can be extrapolated to other types of GBs in Si.

This paper is organized as follows: In Sec. II the computational DFT methods are discussed, and in Sec III the atomistic GB models are described concisely. The results are presented in Sec. IV and are discussed in Sec. V.

## II. COMPUTATIONAL METHODS

All DFT calculations have been carried out using the QUANTUM ESPRESSO PWSCF code [28], which uses a plane-wave basis to represent the wave functions of the valence electrons. Interactions of ionic cores and valence electrons are described by ultrasoft pseudopotentials. The Perdew-Burke-Ernzerhof (PBE) generalized gradient approximation was used

*Benedikt.Ziebarth@iwm.fraunhofer.de

 ©2015 American Physical Society

CSI v. Maxeon, IPR2024-01038 | Maxeon Ex. 2030

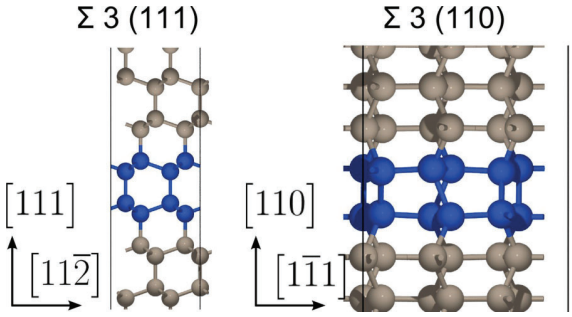


FIG. 1. (Color online) Supercell models of a symmetric tilt GB Σ 3 (111) and a symmetric twist GB Σ 3 (110). Due to periodic boundary conditions, there are two equivalent GBs in the supercells, but for clarity only half of the supercells are shown, with blue atoms highlighting the GB. Tripods indicate the crystallographic directions of the cubic diamond structure.

for exchange correlation [29,30]. All calculations in which Fe was involved were spin polarized. Energy cutoffs of 35 and 350 Ry for the plane-wave basis and the Fourier representation of the electron density, respectively, were found to yield sufficiently converged results. The Brillouin-zone integrals were sampled by Monkhorst-Pack $k$-point grids [31]. The specific grids differ for the various supercells but were checked for equally good convergence in all cases. Atom positions were relaxed until the residual forces acting on them were less than $10^{-4}$ eV/Å. The volume was relaxed for each GB supercell of Si without Fe and was then kept fixed when Fe was inserted at interstitial sites.

## III. GRAIN-BOUNDARY MODELS

Models for a set of coincidence-site-lattice GBs of types Σ 3, Σ 5, and Σ 9 were created. These GBs differ by the inclination of their GB plane and their local atomic configurations. The GB models were selected from low-energy structures of various computational studies and according to experimental observations. Details for the specific GBs are given in the following and in Sec. V.

Figure 1 shows two Σ 3 GBs which differ in their interface planes. The supercells contain 96 and 72 Si atoms for Σ 3 (111) and Σ 3 (110), respectively. The Σ 3 (111) GB is a symmetric tilt GB with its [112] tilt axis lying in the GB plane. The Σ 3 (110) GB is a symmetric twist GB because the twist [112] axis is perpendicular to the GB plane. All Si atoms in these two GB models are fourfold coordinated. The Σ 3 (111) GB has been observed in many experiments (see, e.g., Ref. [19]).

Figure 2 shows the supercell models of another type of the Σ 3 GB, namely, Σ 3 (112). High resolution transmission electron microscopy (HRTEM) investigations [21] showed that this GB can exist in at least two variants, termed the mirror-symmetric and nonsymmetric models.

The two structures differ in reconstructions of the Si bonds along the [112] direction, as indicated by the red bond in Fig. 2. Fivefold-coordinated Si atoms exist in the mirror-symmetric model, whereas all Si atoms are fourfold coordinated in the nonsymmetric model. The supercells contain 136 and 144 Si atoms for the nonsymmetric and mirror-symmetric models, respectively. The reconstructed GB consists of a series of five-, seven-, and sixfold Si rings which are indicated by yellow polygons in Fig. 2.

Finally, Fig. 3 shows the supercell models of three GBs with higher Σ values: Σ 5 (120), Σ 5 (130), and Σ 9 (221). All Si atoms are fourfold coordinated in these GB models. While the Σ 5 (120) and Σ 9 (221) GB interfaces are following a nonsymmetric pattern, the interface of the Σ 5 (130) GB is planar. While the interface structures of the Σ 5 GBs are built from three-, four-, and fivefold Si rings, the interface structure of Σ 9 (221) consists of only five- and sevenfold Si rings. The supercells contain 80, 40, and 136 Si atoms for the Σ 5 (120), Σ 5 (130), and Σ 9 (221) models, respectively. The structures of the chosen Σ 5 GBs have been reported in the literature to be low in energy [32–37]. To our knowledge, no theoretical first-principles study of the Σ 9 (221) GB has been reported so far, but our results for its interface structure is in agreement with experimental HRTEM observations [20].

## IV. RESULTS

### A. Grain-boundary energies

Interface energies $\gamma_{\mathrm{GB}}$ for all GBs are defined as

$$\gamma_{\mathrm{GB}} = \frac{E_{\mathrm{GB}} - N_{\mathrm{Si}}\mu_{\mathrm{Si}}}{2A_{\mathrm{GB}}},$$

where $E_{\mathrm{GB}}$ is the total energy of the GB supercell, $N_{\mathrm{Si}}$ is the number of Si atoms, $\mu_{\mathrm{Si}}$ is the chemical potential of Si, i.e., the total energy of a Si atom in the equilibrium diamond structure,

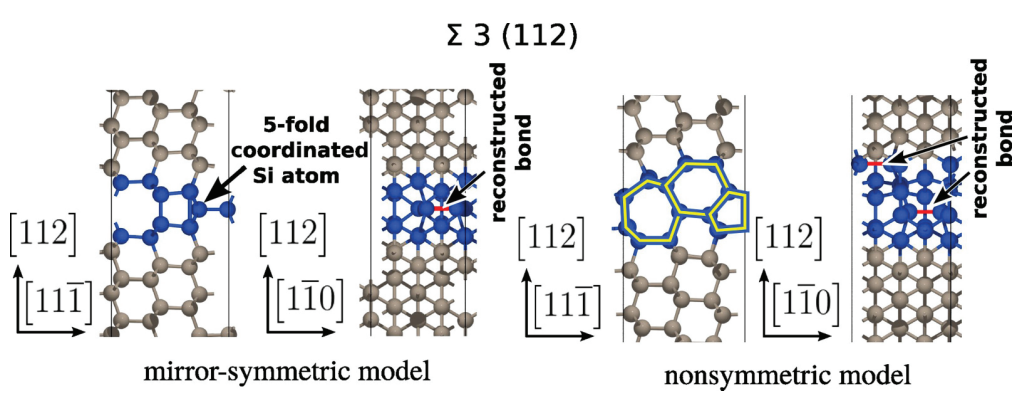


FIG. 2. (Color online) Supercell models of two variants of symmetric tilt Σ 3 (112) GBs.

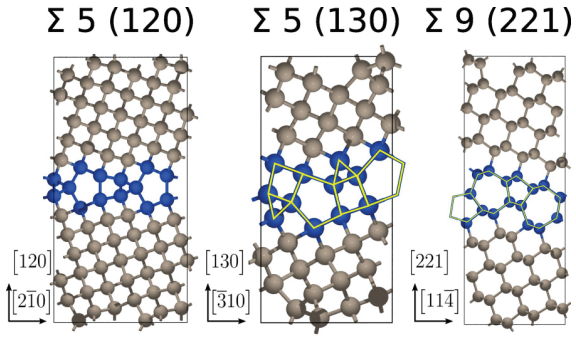


FIG. 3. (Color online) Supercell models of three symmetric tilt GBs: Σ 5 (120), Σ 5 (130), and Σ 9 (221).

and $A_{\mathrm{GB}}$ is the interface area of the GB. The factor of 2 in the denominator takes into account that there are always two grain boundaries in the supercells due to periodic boundary conditions.

The results for GB energies are listed in Table I. As expected, the Σ 3 (111) GB has a very low energy of 0.01 J/m$^2$. The results also indicate that the nonsymmetric reconstruction of the Σ 3 (112) GB leads to a reduction of the GB energy from 0.67 to 0.47 J/m$^2$.

Both Σ 5 GBs are similar in energy in spite of their clearly different geometric arrangements. The Σ 3 (110) GB has the highest energy of 0.76 J/m$^2$. The second-lowest energy of all investigated structures, about 0.16 J/m$^2$, is found for the Σ 9 (221) GB.

### B. Segregation of interstitial iron

After optimization of the GB supercells for pure Si, a single Fe impurity was inserted into various interstitial sites both in the vicinity of the GBs and in the bulklike regions of the models. One of the two Si GBs in the supercell was always populated with Fe. In order to keep the number of calculations feasible we considered only charge-neutral Fe$^{(0)}$ interstitials. Segregation energies of the interstitial Fe atoms at GBs were calculated according to

$$E_{\mathrm{Fe}}^{\mathrm{seg}} = E^{\mathrm{tot}} - \gamma_{\mathrm{GB}} 2 A_{\mathrm{GB}} - N_{\mathrm{Fe}} \mu_{\mathrm{Fe}_i}, \qquad (1)$$

where $E^{\mathrm{tot}}$ is the total energy of a Si GB supercell with an Fe impurity, $N_{\mathrm{Fe}}$ is the number of Fe atoms in the supercell, and $\mu_{\mathrm{Fe}_i}$ is the chemical potential, which is set to the total energy of interstitial Fe in bulk Si, calculated with a cubic supercell containing 64 Si atoms and a single interstitial Fe atom. In addition, we validated that our results are very consistent by comparing the segregation energy of Fe in the bulklike regions of the GB supercell models with that of Fe in the 64-atom bulk-Si supercell.

TABLE I. Calculated GB energies.

| Grain boundary | GB energy (J/m$^2$) | GB energy (meV/Å$^2$) |
|---|---|---|
| Σ 3 (111) | 0.01 | 0.6 |
| Σ 3 (112) symmetric | 0.67 | 41.8 |
| Σ 3 (112) nonsymmetric | 0.47 | 29.3 |
| Σ 3 (110) | 0.76 | 47.4 |
| Σ 5 (120) | 0.39 | 24.3 |
| Σ 5 (130) | 0.35 | 21.8 |
| Σ 9 (221) | 0.16 | 10.0 |

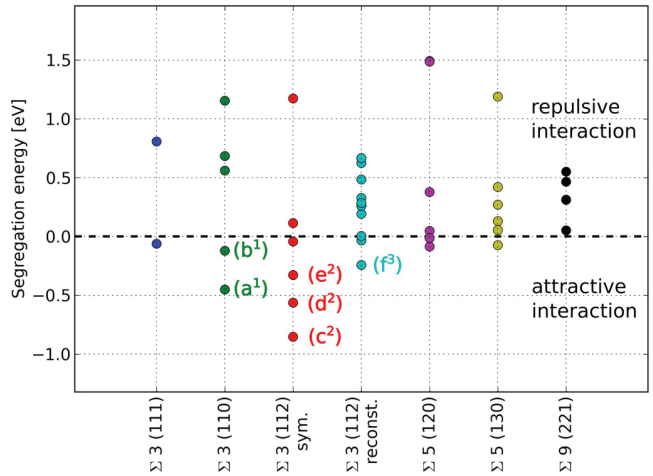


FIG. 4. (Color online) Segregation energies for various interstitial Fe within a 4–8 Å broad region around the GB. For the labeled structures more details are shown in Fig. 5.

We investigated more than 50 interstitial sites in the considered GBs. The segregation energies of unique configurations are shown in Fig. 4. Negative segregation-energy values correspond to an attraction between the GB and Fe; positive values indicate that segregation is not favorable. Sites for which Fe segregation is favorable are labeled (a$^1$) to (f$^3$), where the superscript marks the type of the GB: 1 for Σ 3 (110), 2 for mirror-symmetric Σ 3 (112), and 3 for nonsymmetric Σ 3 (112). These sites will be studied in detail below. Sites with segregation energies larger than −0.1 eV are not considered to attract Fe atoms significantly.

We attempted to correlate several geometric features of the segregation sites (e.g., coordination number, mean bond length, bond angle distribution, and so on) with the segregation energy but were not able to identify any clear relation.

From Fig. 4, it is evident that only three of the investigated GBs show a significantly attractive behavior for interstitial Fe, namely, the two Σ 3 (112) GBs and the Σ 3 (110) GB.

In Fig. 5, the local atomic arrangement of interstitial sites are displayed. The local structures of the (a$^1$) and (b$^1$) sites in the Σ 3 (110) GB are very similar. They differ only in two Si atoms, which are nearby in (a$^1$) but are separated in (b$^1$). In the case of the symmetric model of the Σ 3 (112) GB the (c$^2$) and (e$^2$) sites differ only by their location in the reconstructed GB structure: while one site is located at the reconstructed Si-Si bond, the other site is in the more open environment. Site (d$^2$) closely resembles the tetrahedral position in bulk Si but with one additional Si neighbor giving it a fivefold coordination. Site (f$^3$) of the reconstructed Σ 3 (112) GB is formed by a slightly disturbed sixfold Si ring.

Figure 6 shows the site-projected densities of electronic states (PDOS) for all interstitial configurations depicted in Fig. 5. The PDOS of interstitial Fe in bulk Si has been added as a reference. In bulk Si, interstitial Fe atoms occupy

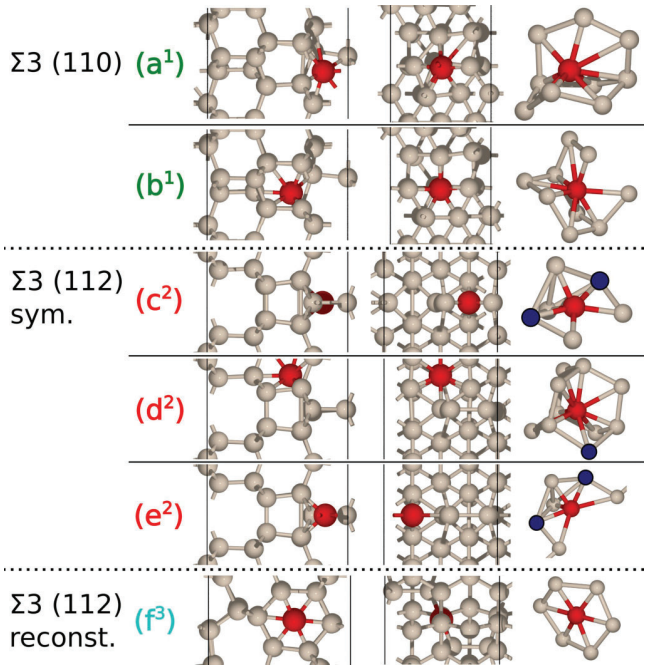


FIG. 5. (Color online) Low-energy configurations of segregated Fe at GBs (see Fig. 4). The structures of the left colum show the site along the $[1\bar{1}0]$ direction, while the pictures in middle column are along the $[111]$ direction. The right column shows the interstitial Fe with its surrounding only. Red spheres are Fe atoms, and blue spheres indicate Si atoms with five Si neighbors.

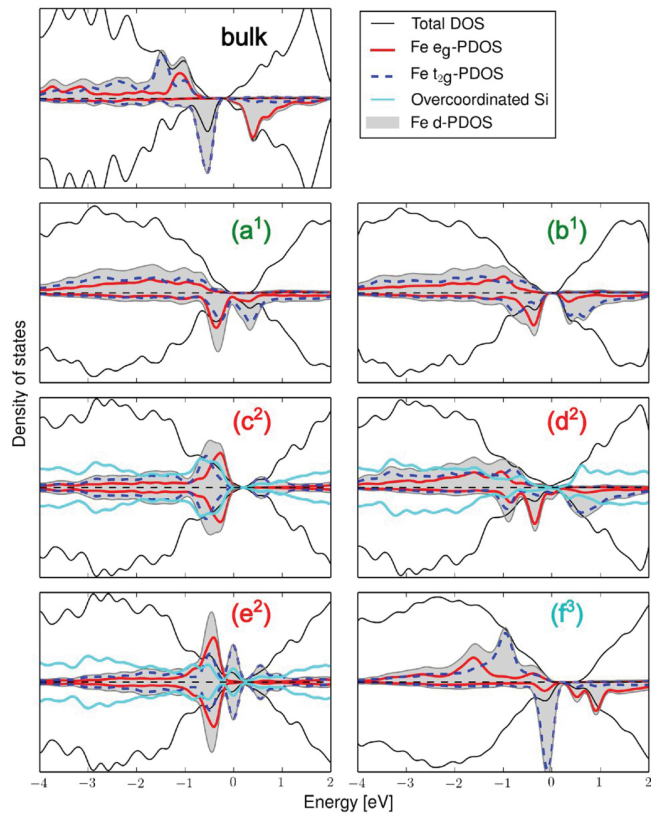


FIG. 6. (Color online) Total and local (site- and orbital-projected) densities of states for the various important segregation sites of interstitial Fe impurities at Si GBs depicted in Figs. 4 and 5. The energy is given with respect to the Fermi energy.

the tetrahedral sites formed by the nearest-neighbor shell of Si atoms. The second-nearest-neighbor shell of Si atoms provide an octahedral coordination. In this bulk interstitial configuration, the Fe 4*s* states are shifted to higher energies above the Fermi energy, and hence, the two 4*s* electrons are transferred into the lower-lying Fe 3*d* states which are thus filled with eight instead of six 4*d* electrons (see the uppermost left panel in Fig. 6). It turns out that the high-spin configuration is favored in bulk Si, i.e., the spin-up *d* states are completely filled by five electrons, and the spin-down *d* states are occupied by three electrons. Due to the cubic crystal-field symmetry, the 3*d* impurity level splits into $t_{2g}$ and $e_g$ levels. However, the crystal-field contribution from the first-nearest neighbors (tetrahedral coordination), which would result in more stable $e_g$ bands, is apparently less effective than the crystal-field contribution from the second-nearest neighbors (octahedral coordination). In accordance with previous investigations, we find that the $t_{2g}$ levels lie lower in energy than the $e_g$ levels [26].

The spin-polarized state of the interstitial Fe in bulk Si remains stable for all GB structures shown in Fig. 4 except for ($c^2$) and ($e^2$). These two special cases will be analyzed further below.

At the GBs, the bulk-specific coordination pattern of nearest-neighbor tetrahedral coordination and second-nearest-neighbor octahedral coordination is usually no longer present, and hence, the electronic structure of the Fe impurity and its environment changes. The investigated structures can be classified into two different groups.

The first group, ($a^1$), ($b^1$), ($d^2$), and ($f^3$), still favors the high-spin configuration like the interstitial Fe in bulk Si. However, the crystal-field splitting of the *d* levels is distorted: the *d* levels split sometimes into more than two peaks, and the peaks are no longer built up by either $e_g$ or $t_{2g}$ levels but by a mixture of the two. Interestingly, the resulting electronic structure of the *d* levels (gray shaded area in Fig. 6) is still similar to that of the interstitial Fe at bulk.

The second group of structures, ($d^2$) and ($f^3$), favors the non-spin-polarized configuration. The peaks of the Fe *d* levels overlap with peaks (turquoise) of a Si atom which is located in the nearest-neighbor shell of Fe. This specific Si atom is coordinated by five Si atoms and is marked by blue spheres in Fig. 5. The overlapping electronic states of neighboring atoms indicate the formation of a chemical bond. It is very likely that this effect causes the spin configuration of Fe to change.

From the analysis above, we conclude that the change of the local electronic structure, particularly that of the *d* states, of interstitial Fe atoms at GBs in Si is mainly due to the different local environments. If only fourfold-coordinated Si atoms exist in this environment, the largest effect is due to the presence of the crystal field. Fivefold-coordinated Si can perfectly lead to the formation of Fe-Si bonds that can alter the spin configuration of the interstitial Fe atoms.

## V. DISCUSSION

In order to study the behavior of Fe impurities in polycrystalline Si, atomistic models for seven symmetric GBs in Si were constructed and structurally relaxed, and their interface energies were calculated. The obtained structures for the two Σ 3 (112) GB models are in agreement with reported HRTEM observation by Sakaguchi *et al.* [21]. Experimentally, the mirror-symmetric arrangement of the GB was apparently found mainly in the vicinity of triple lines of GBs, whereas the nonsymmetric arrangement was observed in GB segments which were free from any other structural distortion. Sakaguchi *et al.* also reported GB energies for the two Σ 3 (112) GB models from their first-principles calculations, namely, 0.56 $J/m^2$ for the nonsymmetric model and 0.75 $J/m^2$ for the mirror-symmetric model, which are in good agreement with our values of about 0.47 and 0.67 $J/m^2$, respectively.

The results of recent first-principles studies for the Σ 5 (130) GB [34,36] also agree well with our data. Our GB energy of 0.35 $J/m^2$ for the Σ 3 (112) GB is close to the values reported by Huang *et al.* (0.38 $J/m^2$) [34], Shi *et al.* (0.37 $J/m^2$) [33], and Lazebnykh and Mysovsky (0.29 $J/m^2$) [36]. We are not aware of any reports of atomistic studies for the Σ 5 (120) and Σ 3 (110) GBs. Our proposed models of the latter two GBs have GB energies similar to those of the other investigated GBs, and hence, we believe that such a GB configuration could exist in Si. We are confident that the chosen set of seven GB models is realistic, representative, and useful for studying the GB segregation of Fe impurities.

The Fe atoms were introduced at interstitial sites of the GBs. Among the seven GB models, an attraction of Fe atoms is found for only three of them, namely, for both models of Σ 3 (112) and Σ 3 (110). This is in agreement with experimental SEM, HRTEM, and EBIC observations. Chen *et al.* showed that in terms of Fe gettering the Σ 3 (111) GB behaves differently from the Σ 3 (112) and Σ 3 (110) GBs [19]. While the latter two GBs strongly attract Fe, the Σ 3 (111) GB does not show Fe segregation at all. The different behaviors of symmetric Σ 3 (111) and Σ 3 (110) GBs was recently confirmed by Nacke *et al.* [38]. Chen *et al.* also reported that individual Fe atoms could be seen at the Σ 3 (112) GB in HRTEM [19]. This is also reflected by our results since some but not all of the interstitial sites are apparently attractive. At odds with our present results, Chen *et al.* reported that the Σ 9 GBs also tend to attract Fe atoms. However, the interface plane orientation was not given for this Σ 9 GB. We therefore cannot be certain whether the Σ 9 GBs which were investigated by Chen *et al.* have the (221) interface plane or a different one.

Two first-principles studies of Fe segregation at individual Si GBs have been reported in the literature: the Σ 3 (111) GB was studied by Suvitha *et al.* [39], and the Σ 5 (130) GB was investigated by Shi *et al.*[33]. The results of both studies for the segregation energies are in agreement with our results within 0.1 eV. Shi *et al.* also tried to correlate the local geometric arrangement of the Si atoms at the segregation sites with the segregation energy of Fe. Like us, they concluded that it was not possible to identify any clear trend.

Our results indicate that, in particular, the symmetric Σ 3 (112) GB is a very favorable interface for Fe segregation. This may partially be attributed to the existence of fivefold-coordinated Si atoms at the GB. The segregated Fe atoms create a chemical bond with such Si atoms and thereby lower the energy. Such local bonding was indicated in the PDOS curves (see Fig. 6). Therefore, it is likely that intrinsic defects at GBs, such as Si atoms, that are not fourfold coordinated may trap Fe and even create chemical bonds between the Si and Fe atoms. It is known that Fe forms Fe silicide precipitates at GBs in Si, and hence, such an initial bond may act as a seed for precipitation of Fe-Si particles.

Another observation follows from the calculated DOS in Fig. 6: the electronic structure of interstitial Fe at GBs may differ significantly from that of interstitial Fe in bulk Si. For instance, the Fe atoms at the GB become non-spin-polarized or the Fe *d* states split into more than two levels. This is of particular relevance for experimental detection methods of interstitial Fe which rely on the energy position of the deep defect levels of Fe in the band gap, for instance, $\mu$-PL [16]. This position may vary for different GBs in Si, and therefore, segregated interstitial Fe may not be detected properly by such methods. In all cases a deep level from an Fe impurity remains in the band gap of Si, and hence, a previously inactive Fe-free GB in Si can become electrically active upon Fe segregation. If segregated Fe atoms accumulate and form Fe-Si precipitates at the GB, a bandlike electronic state can develop instead of a single deep level. This is relevant for experimental methods such as deep-level transient spectroscopy [40].

Our study was performed under the assumption that Fe atoms occupy interstitial positions at GBs. It cannot be excluded that Fe atoms also substitute for Si atoms at the GB. In bulk Si, interstitial Fe atoms occupy Si vacancies and become substitutional defects [41], but Si vacancies are very unlikely in bulk Si because they have large formation energies. However, this formation energy of Si vacancies is smaller at GBs; that is, Si vacancies are attracted by GBs [36,42,43]. The possibility for Fe to occupy Si vacancies at the GB sites may therefore be more likely than in bulk Si. GBs also attract other impurity elements [42,44–47] that can modify the segregation behavior of Fe at the GB.

In addition to the considered low-Σ and large-angle GBs, there are random GBs and high-Σ and small-angle GBs as well, which all show a very strong attraction for the Fe atoms [18,48]. It is likely that random GBs incorporate a large variety of Si defects characterized by over- or undercoordinated Si atoms and/or large distortions of bond angles and bond lengths. The strong segregation can be explained by the interaction of Fe atoms with these defect arrangements at the GB, similar to what was observed here for the symmetric Σ 3 (112) GB. The situation is different for small-angle GBs. This type of GB is composed of periodic interfacial Read-Shockley dislocation arrangements with no overlapping dislocation cores [49]. It is known that dislocations tend to reconstruct along their dislocation lines [50] and thereby avoid over- or undercoordinated Si sites. However, both bulk and GB dislocations have elastic strain fields surrounding them, which may affect the segregation behavior of Fe atoms [18,38,51]. An elastic strain field is also observed around GBs which contain Fe precipitates [18,19,38]. However, in this case it is not evident whether the strain field is induced by the growth of the precipitate at the GB or it is present beforehand.

In further studies it will become necessary to extend the calculations of Fe segregation at Si GBs to small-angle GBs and random GBs. Atomistic structures of these GBs require large supercell models or even nonperiodic models. First-principles calculations will become unfeasible at this stage, and simplified but sufficiently accurate models for the Fe-Si interaction, such as tight-binding Hamiltonians or empirical interactive potentials, need to be developed. Our present study provides benchmark data for the development of such models.

So far, the properties of Fe impurities in bulk Si have been studied in the most detail, and little effort has been spent on extending the knowledge of the interactions between Fe impurities and extended defects in Si on an atomic scale. However, this interaction is of great importance for photovoltaic applications of polycrystalline Si as GBs and dislocations are abundant in this material.

## VI. CONCLUSION

In order to reduce the detrimental effect of Fe impurities in mc-Si solar cells, internal gettering exploits the interaction between Si GBs and Fe impurities. To this end, the segregation of interstitial Fe at a set of low-Σ GBs in Si was studied by means of density functional theory. Preferred segregation of Fe with segregation energies ranging between 0.2 and 0.8 eV was found for two variants of the Σ 3 (112) GBs and for the Σ 3 (110) GB. None of the other considered GBs, i.e., Σ 3 (110), Σ 5 (120), Σ 5 (130), and Σ 9 (221), showed significant attraction of Fe. Moreover, the simple geometric feature of the local structure of the interstitial site does not simply correlate with segregation energies. Hence, the mechanism which determines the thermodynamics of Fe at GBs remains an open question. In addition to that, the electronic structures of the available segregation sites were studied in detail. In most cases the spin configuration of Fe at the GB is the same as that for Fe in bulk Si. However, in some cases we observed a large change in the electronic structure of Fe at the GB, and hence, Fe atoms at GBs might not be detected properly by experiments. This study contributes to a better understanding of the underlying atomistic mechanism of Fe segregation at GBs in Si. This can be useful for both the interpretation of experimental observation and the improvement of processing techniques to passivate Fe impurities in polycrystalline Si wafers for photovoltaic applications.

## ACKNOWLEDGMENTS

This work was funded by the Hans L. Merkle foundation of Robert Bosch GmbH. Computer resources at the Steinbuch Centre for Computing of the Karlsruher Institut für Technologie are gratefully acknowledged.

[1] S. Pizzini, M. Acciarri, and S. Binetti, Phys. Status Solidi A **202**, 2928 (2005).
[2] A. Istratov, H. Hieslmair, and E. Weber, Appl. Phys. A **69**, 13 (1999).
[3] A. Istratov, H. Hieslmair, and E. Weber, Appl. Phys. A **70**, 489 (2000).
[4] G. Coletti, P. C. Bronsveld, G. Hahn, W. Warta, D. Macdonald, B. Ceccaroli, K. Wambach, N. Le Quang, and J. M. Fernandez, Adv. Funct. Mater. **21**, 879 (2011).
[5] T. Buonassisi, A. A. Istratov, M. D. Pickett, M. Heuer, J. P. Kalejs, G. Hahn, M. A. Marcus, B. Lai, Z. Cai, S. M. Heald, T. F. Ciszek, R. F. Clark, D. W. Cunningham, A. M. Gabor, R. Jonczyk, S. Narayanan, E. Sauar, and E. R. Weber, Prog. Photovoltaics **14**, 513 (2006).
[6] D. Macdonald and L. Geerligs, Appl. Phys. Lett. **85**, 4061 (2004).
[7] A. Hähnel, J. Bauer, H. Blumtritt, O. Breitenstein, D. Lausch, and W. Kwapil, J. Appl. Phys. **113**, 044505 (2013).
[8] A. Istratov, T. Buonassisi, M. Pickett, M. Heuer, and E. Weber, Mater. Sci. Eng. B **134**, 282 (2006).
[9] A. Liu, D. Walter, S. P. Phang, and D. Macdonald, IEEE J. Photovoltaics **2**, 479 (2012).
[10] A. Y. Liu, D. Walter, S. P. Phang, and D. Macdonald, in *38th IEEE Proceedings on Photovoltaic Specialists Conference (PVSC), 2012* (IEEE, Piscataway, NJ, 2012), pp. 000248–000253.
[11] D. Macdonald, A. Y. Liu, and S. P. Phang, Solid State Phenom. **205**, 26 (2014).
[12] J. Hofstetter, D. P. Fenning, D. M. Powell, A. E. Morishige, and T. Buonassisi, Solid State Phenom. **205**, 15 (2014).
[13] M. Seibt and V. Kveder, *Gettering Processes and the Role of Extended Defects* (Wiley, Hobokne, NJ, 2012), pp. 127–188.
[14] A. Liu, Y.-C. Fan, and D. Macdonald, Prog. Photovoltaics **19**, 649 (2011).
[15] D. Macdonald, J. Tan, and T. Trupke, J. Appl. Phys. **103**, 73710 (2008).
[16] M. C. Schubert, H. Habenicht, and W. Warta, IEEE J. Photovoltaics **1**, 168 (2011).
[17] J. Chen, T. Sekiguchi, D. Yang, F. Yin, K. Kido, and S. Tsurekawa, J. Appl. Phys. **96**, 5490 (2004).
[18] J. Chen, T. Sekiguchi, R. Xie, P. Ahmet, T. Chikyo, D. Yang, S. Ito, and F. Yin, Scr. Mater. **52**, 1211 (2005).
[19] J. Chen, B. Chen, W. Lee, M. Fukuzawa, M. Yamada, and T. Sekiguchi, Solid State Phenom. **156–158**, 19 (2009).
[20] J. Thibault, J.-L. Putaux, A. Jacques, A. George, and M. Elkajbaji, Microsc. Microanal. Microstruct. **1**, 395 (1990).
[21] N. Sakaguchi, H. Ichinose, and S. Watanabe, Mater. Trans. **48**, 2585 (2007).
[22] J. Chen, D. Yang, Z. Xi, and T. Sekiguchi, J. Appl. Phys. **97**, 033701 (2005).
[23] A. P. Sutton and R. W. Balluffi, *Interfaces in Crystalline Materials* (Clarendon, Oxford, 1995).
[24] M. Knörlein, A. Autruffe, R. Søndenå, and M. Di Sabatino, Energy Procedia **55**, 539 (2014).
[25] M. Sanati, N. G. Szwacki, and S. K. Estreicher, Phys. Rev. B **76**, 125204 (2007).
[26] G. W. Ludwig and H. H. Woodbury, Phys. Rev. Lett. **5**, 98 (1960).
[27] H. H. Woodbury and G. W. Ludwig, Phys. Rev. **117**, 102 (1960).
[28] P. Giannozzi *et al.*, J. Phys. Condens. Matter **21**, 395502 (2009).

[29] D. Vanderbilt, Phys. Rev. B **41**, 7892 (1990).
[30] J. P. Perdew, K. Burke, and M. Ernzerhof, Phys. Rev. Lett. **77**, 3865 (1996).
[31] H. Monkhorst and J. Pack, Phys. Rev. B **13**, 5188 (1976).
[32] J. Zhang, C.-Z. Wang, and K.-M. Ho, Phys. Rev. B **80**, 174102 (2009).
[33] T. Shi, Y. Li, Z. Ma, G. Qu, F. Hong, F. Xu, Y. Yan, and S.-H. Wei, J. Appl. Phys. **107**, 093713 (2010).
[34] W. L. Huang, W. Ge, C. Li, C. Hou, X. Wang, and X. He, Comput. Mater. Sci. **58**, 38 (2012).
[35] V. Y. Lazebnych and A. Mysovsky, Phys. Solid State **54**, 2357 (2012).
[36] V. Y. Lazebnykh and A. S. Mysovsky, arXiv:1308.3802.
[37] M. Kohyama, Modell. Simul. Mater. Sci. Eng. **10**, R31 (2002).
[38] M. Nacke, M. Allardt, P. Chekhonin, E. Hieckmann, W. Skrotzki, and J. Weber, J. Appl. Phys. **115**, 163511 (2014).
[39] A. Suvitha, N. S. Venkataramanan, R. Sahara, H. Mizuseki, and Y. Kawazoe, Jpn. J. Appl. Phys. **49**, 04DP02 (2010).
[40] M. Seibt, R. Khalil, V. Kveder, and W. Schröter, Appl. Phys. A **96**, 235 (2009).
[41] S. K. Estreicher, M. Sanati, and N. Gonzalez Szwacki, Phys. Rev. B **77**, 125214 (2008).
[42] V. Lazebnykh and A. Mysovsky, JETP Lett. **98**, 76 (2013).
[43] C. B. Feng, J. L. Nie, X. T. Zu, M. M. Al-Jassim, and Y. Yan, J. Appl. Phys. **106**, 113506 (2009).
[44] J. Schön, H. Habenicht, W. Warta, and M. C. Schubert, Prog. Photovoltaics **21**, 676 (2013).
[45] J.-L. Maurice and C. Colliex, Appl. Phys. Lett. **55**, 241 (1989).
[46] M. F. Chisholm, A. Maiti, S. J. Pennycook, and S. T. Pantelides, Phys. Rev. Lett. **81**, 132 (1998).
[47] M. M. Mandurah, K. C. Saraswat, C. R. Helms, and T. I. Kamins, J. Appl. Phys. **51**, 5755 (1980).
[48] Y. Miyamura, H. Harada, S. Ito, J. Chen, and T. Sekiguchi, Mater. Sci. Forum **725**, 157 (2012).
[49] W. Read and W. Shockley, Phys. Rev. **78**, 275 (1950).
[50] J. Rabier, L. Pizzagalli, and J. Demenet, in *Dislocations in Solids* (Elsevier, Amsterdam, 2010), Vol. 16, pp. 47–108.
[51] K. Suzuki, Y. Yoshida, T. Kamimura, M. Ichino, and K. Asahi, Phys. B (Amsterdam, Neth.) **404**, 4678 (2009).